Electrocatalysis (2021) 12:564–578
https://doi.org/10.1007/s12678-021-00669-4

ORIGINAL RESEARCH

Mixed Lithium and Sodium Ion Aprotic DMSO Electrolytes for Oxygen Reduction on Au and Pt Studied by DEMS and RRDE

M. Hegemann[1] · P. P. Bawol[1] · A. Köllisch-Mirbach[1] · H. Baltruschat[1]

Accepted: 25 April 2021 / Published online: 15 May 2021

Abstract

In order to advance the development of metal-air batteries and solve possible problems, it is necessary to gain a fundamental understanding of the underlying reaction mechanisms. In this study we investigate the oxygen reduction reaction (ORR) and oxygen evolution reaction (OER, from species formed during ORR) in Na^+ containing dimethyl sulfoxide (DMSO) on poly and single crystalline Pt and Au electrodes. Using a rotating ring disk electrode (RRDE) generator collector setup and additional differential electrochemical mass spectrometry (DEMS), we investigate the ORR mechanism and product distribution. We found that the formation of adsorbed Na_2O_2, which inhibits further oxygen reduction, is kinetically favored on Pt overadsorption on Au. Peroxide formation occurs to a smaller extent on the single crystal electrodes of Pt than on the polycrystalline surface. Utilizing two different approaches, we were able to calculate the heterogeneous rate constants of the O_2/O_2^- redox couple on Pt and Au and found a higher rate for Pt electrodes compared to Au. We will show that on both electrodes the first electron transfer (formation of superoxide) is the rate-determining step in the reaction mechanism. Small amounts of added Li^+ in the electrolyte reduce the reversibility of the O_2/O_2^- redox couples due to faster and more efficient blocking of the electrode by peroxide. Another effect is the positive potential shift of the peroxide formation on both electrodes. The reaction rate of the peroxide formation on the Au electrode increases when increasing the Li^+ content in the electrolyte, whereas it remains unaffected on the Pt electrode. However, we can show that the mixed electrolytes promote the activity of peroxide oxidation on the Pt electrode compared to a pure Li^+ electrolyte. Overall, we found that the addition of Li^+ leads to a Li^+-dominated mechanism (ORR onset and product distribution) as soon as the Li^+ concentration exceeds the oxygen concentration.

Keywords Oxygen reduction reaction · Metal-air-batteries · RRDE study · Rate constants in Na^+ electrolyte Li^+ · Na^+ mixed electrolytes

Introduction

For the solution of the energy storage problem, the Li/Air battery is being discussed as an attractive alternative by various researchers. The Li/Air system has a high practical energy density (theo. energy density: 3458 Wh kg^{-1} (Li_2O_2) [1]), which is comparable to gasoline [2]. In the Li/Air system, the oxygen reduction reaction (ORR) forms first lithium superoxide (LiO_2) which is soluble and afterward lithium peroxide (Li_2O_2). Li_2O_2 can be reoxidized which ends in the oxygen evolution reaction (OER), but the coulombic efficiency/electrochemical reversibility (OER/ORR) is less than 100% [3, 4]. The equations shown in Table 1 are possible reaction products in the Li/Air system for the ORR reaction.

Using the tabulated potential values by Gritzner [7], Table 1 also gives potential values referred to the $Ag|Ag^+$ which is used in this study. Because of the limiting availability of lithium, researchers are thinking about other alkali metal–oxygen batteries [8–11]. These have the same working principle like the Li/Air system, but the anode material is changed. The next attractive battery system is the Na/Air system, because of the abundant sodium source, low manufacturing costs, environmental benignity, high capacity, and a high theoretical energy density of 1108 Wh kg^{-1} (NaO_2) [1, 12]. Peled et al. showed 2011 for the first time that a sodium-air battery, using 1 M $NaClO_4$ with 1% Al_2O_3

✉ H. Baltruschat
baltruschat@uni-bonn.de

[1] Institute for Physical and Theoretical Chemistry, University of Bonn, Römerstr. 164, 53117 Bonn, Germany

Table 1 Standard electrode potentials for the possible products

Reaction	Metal	E^0 vs. M/M^+	E^0 vs. Ag/Ag^+	ΔG
$M + O_2 \rightarrow MO_2$	Li	3.0 V	− 0.84 V	− 293 kJ mol^{-1} [5]
$2M + O_2 \rightarrow M_2O_2$	Li	3.1 V	− 0.74 V	− 607 kJ mol^{-1} [5]
$4M + O_2 \rightarrow 2M_2O$	Li	2.91 V	− 0,93 V	− 1121 kJ mol^{-1} [5]
$M + O_2 \rightarrow MO_2$	Na	2.26 V	− 1.03 V	− 218.4 kJ mol^{-1} [6]
$2M + O_2 \rightarrow M_2O_2$	Na	2.33 V	− 0.97 V	− 449.6 kJ mol^{-1} [6]
$4M + O_2 \rightarrow 2M_2O$	Na	1.95 V	− 1.34 V	− 751 kJ mol^{-1} [6]

dispersed in polyethylene-glycol-dimethyl ether in propylenecarbonate (polymer electrolytes) on Au electrodes, which is running above 100 °C, is a promising alternative battery to the actual lithium-ion batteries [13]. This cell had a faradaic efficiency of 85%. Ellis et al. showed in 2012 the possible reduction products of the ORR in Na^+-containing carbonate electrolytes [14].

Further studies focused on ether [15–21] and carbonate [6, 17, 18] based electrolytes, while it was found that the underlying mechanism depends on the solvent [17]. Also, Aldous et al. showed that by SERS measurements, the solvent controls the formation of the discharge products [22]. Bender et al. showed in 2014 using thermodynamic data that in ether-based electrolytes, the formation of NaO_2 together with Na_2O_2 is favorable, but the formation of Na_2O is thermodynamically unfavorable [18]. They also studied carbon-based electrolytes and found as main product NaO_2 in their cell design. Schröder et al. used in 2016 three different electrochemical and chemical ways to form Na_2O_2 on Au electrodes, but the main product of each pathway is NaO_2 [23]. Via a theoretical approach, it was found that under standard conditions, Na_2O_2 is stable and NaO_2 is metastable, but the partial pressure of O_2 is a significant parameter to determine the formation and growth of a particular sodium oxide phase [24]. Whether the one- or a two-electron process is occurring is still an open question in the Na-O_2 cells [25].

Landa-Medrano et al. mixed 2018 Li^+ and K^+ salts to a sodium-containing diglyme electrolyte [26]. By mixing Li^+ to the Na^+ electrolyte, the stabilization of O_2^- is hindered in the electrolyte and a surface-phase ORR is favored, and therefore, an early accumulation of the discharge products occurs. The increase of K^+ in the Na^+ electrolyte resulted in a reduced overpotential for ORR and OER.

Bondue et al. focused 2015 on the ORR and OER in DMSO-based electrolytes [27]. They used different electrode materials and different cations in the solvent DMSO. Using DEMS, they found on Au electrode in the sodium containing electrolyte a transition from the $1e^-$ per O_2 process to the 2 e^- per O_2 process with increasing overpotential. On the Pt electrode, the transferred electron number passes a maximum of 1.5 e^- per O_2. Dilimon et al. focused on the stability of superoxide in the combination of different sodium salts in DMSO [28]. They found that the ClO_4^-/DMSO electrolyte leads to a stable superoxide product during ORR. The Na_2O_2 is just formed by a second ORR step of electrochemical two-electron reduction of molecular oxygen to peroxide. In PF_6^-/DMSO, the formed superoxide disproportionates to the surface adsorbed peroxide. Ma et al. investigated oxygen reduction in a $NaClO_4$/DMSO electrolyte by CV, in situ SERS and DFT-based theoretical modeling [29]. Their findings suggest that the passivation of the cathode surface can be avoided in low-overpotential regime, because NaO_2 is slightly soluble in the DMSO electrolyte. They measured the solubility product of NaO_2 with UV–Vis-spectroscopy and found a value of $7.95 \cdot 10^{-4}$ M assuming dissociation into O_2^- and Na^+ as compared to the much lower solubility of LiO_2 [30].

Sheng et al. studied the disproportionation of sodium superoxide in different solvents [31] and found for both superoxide in solution and on the surface ($NaO_{2(sol)}$ and $NaO_{2(sur)}$) that the disproportionation kinetics to Na_2O_2 depends on the solvent. The disproportionation of $NaO_{2(sol)}$ is fast in acetonitrile but slow in DMSO or diglyme; therefore, the NaO_2 is found as the major discharge product. In DMSO, dissolved NaO_2 accumulates and precipitates, forming flake-shaped particles. The formed Na_2O_2 passivates the surface, and this results in polarization. Both NaO_2 and Na_2O_2 are reactive and would attack electrolytes.

Using EC-SHINERS and cyclic voltammetry for the analysis of the ORR products on Pt(111), Pt(100), and Pt(110) in $NaClO_4$/DMSO electrolyte, Galloway et al. showed that the ORR on platinum is surface specific and that on Pt(110) and Pt(111) the reduction of NaO_2 to Na_2O_2 is promoted, contrary to Pt(100) and polycrystalline Pt [32].

In this study, we are examining the differences in the kinetics of the ORR in Na^+-containing DMSO on Au and Pt electrode using cyclic voltammetry and the rotating ring disc electrode. In addition, the effect of mixed Na^+-Li^+ electrolytes on the ORR and OER is elucidated, thus continuing our studies on the Li-O_2 system [3, 27, 33, 34]. This will shed some light on the different ORR kinetics in Li^+- and Na^+-containing electrolytes. A further motivation for investigating the mixtures of the two different salts was to elucidate the prospects of a battery system, which combines the positive effects of both electrode systems. This means to get a better reversibility than in the pure Li cell, to avoid

the higher amount of singlet oxygen like in the pure Na cell and to enlarge the energy density by adding Li salt [35]. In particular we will show that the potential of peroxide formation is shifting to higher (more negative) overpotentials with increasing Na content.

Experimental

Chemicals

Sodium perchlorate hydrate ($NaClO_4 \cdot H_2O$, Sigma-Aldrich, 99.99% trace metal basis) was dried at 180 °C at reduced pressure for two days. Lithium perchlorate ($LiClO_4$, Sigma-Aldrich, battery grade, dry, 99.99% trace metal basis) was used as received. Dimethyl sulfoxide (DMSO, 99.7%, stored under molecular sieve, Acros Organics, $H_2O < 50$ ppm) was used as received. All electrolytes were prepared in a GS glovebox with a water content below 0.5 ppm. The water content of the electrolytes was determined by Karl-Fischer titration after the experiment and reached values between 30 and 70 ppm. Silver nitrate ($AgNO_3$, ≥ 99%, ChemPure) was used for preparation of the reference electrode, which was a silver wire in a 0.1 M $AgNO_3$ in DMSO. All electrolytes were purged either with a custom mixture of argon and oxygen (80:20, Air Liquide) or with a mixture of highly pure argon (99.9999%, Alphagaz 2, Air Liquide) and highly pure oxygen (99.9995%, Alphagaz 2, Air Liquide). The 80:20 Ar-O_2-mixtures were produced by mixing the above mentioned gases using an electrical flow meters (F-201C-UA-22-V, Bronkhorst, MFT-V12C Union Carbide). The flow meters were calibrated for the specific gases.

Electrode Cleaning

For cleaning, the Pt and Au electrodes were cycled in 0.5 M H_2SO_4 until the well-known CV shape could be observed.

RRDE Setup

The RRDE measurements were performed in a three-electrode arrangement. As electrochemcial cell a three-compartment glass cell with a Luggin-Capillary [36] was used. Electrical contact to the reference electrolyte (0.1 M $AgNO_3$ in DMSO) with the reference electrode (Ag-wire) in one of the compartments was established by the wetted rough surface of a closed glass stopcock. As counter electrode a gold wire was used. As working electrode, a thin-gap RRDE-tip with an Au-disk and an Au-ring (AFE7R8AuAu, Pine Research Instrumentation) and a thin-gap RRDE-tip with a Pt-disk and a Pt-ring (AFE7R8PtPt, Pine Research Instrumentation) were used. The thin gap electrode has a theoretical collection efficiency of $N_0 = 0.22$, and the surface of the disk electrode is $A = 0.164$ cm^2. For the data evaluation, the share of superoxide (X) was calculated. X can be calculated from the ring current I_R and the disk current I_D assuming that only superoxide and peroxide are formed as products and that only superoxide is oxidized at the ring electrode:

$$X = \frac{-2I_R}{(N_0 I_D) - I_R} \tag{1}$$

Furthermore, we want to emphasize that in this study we correct the time offset between the ring current and the disk current. The time offset results from the transfer time of a species that is formed at the disk and is transported to the ring due to the velocity field. At a rotation speed of 4 Hz this can be estimated with 1 s [37]. If the ring current is corrected by the time offset, it can be seen that the peak potentials in the ring current correspond to those in the disk current. Therefore, a coincidence of the peak potentials was used to correct the time offset.

DEMS Setup

The dual thin-layer cell used for DEMS measurements has two compartments, which are connected by six capillaries, and the electrolyte is flushed with 5 µL s^{-1} through the cell by a peristaltic pump, which is connected at the outlet of the cell. In the upper compartment, the electrochemical reaction on the working electrode (Au_{poly}, Pt_{poly}) takes place. The lower compartment is connected with a porous PTFE membrane to the mass spectrometry (MS). Volatile species in the electrolyte can evaporate through the porous PTFE membrane into the vacuum of the mass spectrometer and be detected by the MS. The reference electrode is connected at the inlet. The main counter electrode is placed at the outlet. To reduce electronic oscillations, a second counter electrode is placed at the inlet. For an optimal distribution of the current, a 1 Ω resistance is used at the main counter electrode and 1 MΩ resistance at the second electrode. A more detailed description of the cell can be found elsewhere [38–41]. The DEMS setup is calibrated by using a system in which the ORR is undergoing with a well-known stoichiometry. Therefore, the ORR is performed in a 0.5 M $KClO_4$/DMSO electrolyte in the same cell on the same. It is known that in this electrolyte, the oxygen reduction takes place via a one-electron process in a wide potential window [27, 42]. This allows the calculation of the oxygen flux $\dot{n}(O_2)$ and finally the determination of the number of transferred electrons per oxygen molecule z according to the following equation [10]:

$$z = \frac{I_F}{\dot{n}(O_2)F} \quad (2)$$

Single-Crystal Setup

Experiments in resting solution were conducted in an H-cell using the well-known three-electrode arrangement, with the single crystalline electrodes as working electrode (WE diameter 1 cm; 0.785 cm^2), a silver wire immersed into 0.1 M $AgNO_3$ containing DMSO as reference electrode (RE) and a platinum sheet as counter electrode (CE). CE and WE were separated by a glass frit. The differential electrochemical mass spectrometry experiments were performed with the single crystal electrode in the thin layer DEMS cell as described above.

Preparation of the Single-Crystal Electrodes

The single crystals were cleaned as described above and annealed in an induction heat cell afterward. To obtain a well-ordered (111) or (100) surface, the cell was purged with N_2 in case of Pt(111) and with (95% Ar + 5% H_2) in case of Pt(100) during the annealing procedure (150 s at yellow heat) and also during cooling down of the crystal above Milli-Q water [43, 44]. After cooling down for 10 min, the electrode was protected for transport by adsorbing a monolayer of bromide from a 1 mM KBr solution. Once every day, prior to an experiment, the electrodes were characterized in H_2SO_4 after bromide protection to proof the setup. If the single crystals show their typical CV (see Fig. S1) after stripping of the bromide, the crystals were prepared again, protected, dried in ambient air, and transferred to the experimental setup. This procedure ensures the protection of the well-ordered surfaces against contaminants from ambient air (note that water needs to be avoided for investigations of the ORR in organic electrolytes) similar to [32]. As shown in [45], bromide is stripped in DMSO at −0.61 V vs $Ag|Ag^+$ (prior to the ORR onset), and thus, we can safely assume that the bromine adlayer will not influence the ORR. This is further supported by a current study [46], where we found complete, reductive dissolution of the bromine adlayer (proven with XPS) in DMSO within the first cycle (prior to the ORR onset).

Results and Discussion

The ORR in Na^+-Containing DMSO: a Comparison Between Au and Pt Electrocatalyst

This study aims at a direct comparison of the ORR and OER on the electrocatalysts Pt and Au. Therefore, we start with some fundamental investigations of the ORR and OER using cyclic voltammetry (CV). Figure 1 shows the CVs of a potential window opening experiment in 0.1 M $NaClO_4$ in DMSO saturated with a mixture of 20:80 O_2:Ar recorded on a Pt working electrode (a) and on an Au working electrode (b).

Both sets of CVs show two peaks in the cathodic sweep. The first peak (C_1) is associated with the formation of superoxide and the second peak (C_2) with the formation of peroxide. Variation of the lower potential limit confirms the assignments of the anodic peaks A_2 and A_1 (oxidation of peroxide and superoxide) to the corresponding reverse reactions. This assignment is based on our previous DEMS study

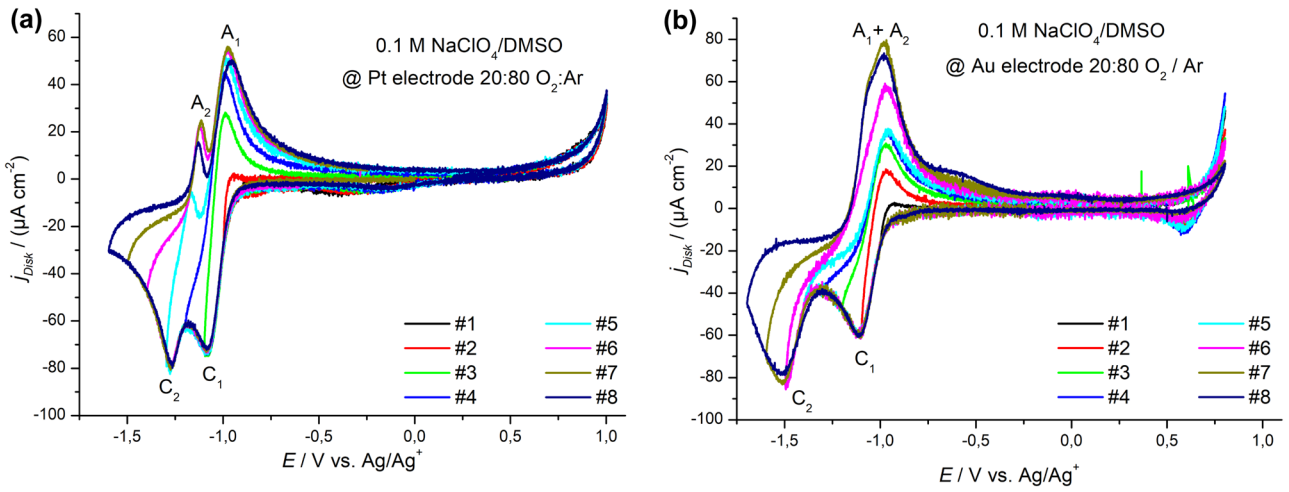

Fig. 1 CV study in 0.1 M $NaClO_4$ in DMSO electrolyte on (**a**) Pt working electrode and (**b**) Au working electrode at a constant sweep rate of 10 mV s^{-1} (A = 0.164 cm^2). The lower potential was reduced in 100 mV steps in every cycle. The electrolyte was saturated with a mixture of 20:80 O_2:Ar

where we quantified the number of electrons transferred per oxygen molecule [27]; a similar DEMS experiment is reproduced in Fig. S2. In comparison to the Li^+ system, the peroxide formation is much more reversible, similar to the K^+-containing system [47]. On both Pt and Au, superoxide formation starts in the onset of ORR (1 e^-/O_2), followed by peroxide formation (2 e^-/O_2). The formation of superoxide occurs on both the Au electrode and the Pt electrode at the same potential ($E_{1/2}(C_1) = -1.0$ V vs. $Ag^+|Ag$). It is noticeable that the peroxide formation on the Pt surface is starting 180 mV more positive than at Au ($E_{1/2}(C_2, Pt) = -1.25$ V vs. $Ag^+|Ag$ and $E_{1/2}(C_2, Au) = -1.43$ V vs. $Ag^+|Ag$). In the anodic sweep, the OER shows two well-separated peaks on the Pt electrode. On the Au electrode, the oxidation of peroxide (A_2) and superoxide (A_1) is not well separated. In this case, the oxidation of peroxide is noticeable as a shoulder in the CV. The dependence on the sweep rate is shown in the supporting information (Fig. S3). The peak current increases linearly with the square root of sweep rate on both electrodes (Randles–Sevcik plot, Fig. S4), which shows diffusion limitation for the first electron transfer. Figure S3 also shows that the peak potentials depend on the sweep rate. This allows a determination of the rate constant for the first electron transfer, as outlined in the supporting information.

A similar experiment at 100% O_2 saturation (Fig. 2) shows a different behavior of Peak A_1 on the Pt electrode: as the potential limit is opened in negative direction, the peak potential of peak A_1 is shifting into positive direction and the peak height is decreasing. We suggest that this effect is due to a complete blocking of the electrode with Na_2O_2, which is only achieved at short times when saturating the electrolyte with 100% O_2. (In Fig. 1, reduction continues in the anodic sweep after potential reversal (with about 2 µA as opposed to Fig. 2a) where a corresponding current should be 5 times larger.) It is reasonable to assume that for an electrode that is completely blocked with a film of ORR products, the first step of the OER is the formation of holes in this film. Oxidation of dissolved ORR products (such as superoxide) can only take place at such holes. Formation of a hole by oxidation is more difficult on a complete film than on an incomplete film because it requires contact between the peroxide, the electrocatalyst and the solution phase and therefore requires a higher overpotential—a typical nucleation phenomenon. This behavior is not observed on Au because of the less strong interaction of the deposited ORR products with the Au surface as compared to Pt. Note that on Au, complete blocking is only achieved at the lowest potential limit; in the anodic sweep, peroxide oxidation (to superoxide) is superimposed to the newly starting O_2 reduction to superoxide on the freed surface. The DEMS experiment (Fig. S2) and also the experiments shown below confirm that roughly a monolayer of Na_2O_2 is formed.

Ma et al. [29] used surface enhanced Raman spectroscopy (SERS) to identify the products formed in these peaks. (The difference between their CV and ours is probably due to the much higher roughness necessary for SERS and the pausing during the potential scan for recording the spectra.) They assigned peak C_1 to the formation of adsorbed superoxide on the Au electrode and peak C_2 to the formation of solid NaO_2 on the electrode surface. Only at the negative potential limit they observed the formation of Na_2O_2 without further charge flowing. This contradicts our previous DEMS study [27] (newly confirmed here in the experiment shown in Fig. S2 in the supporting information), where we show that peak C_2 is associated with peroxide formation. We believe that the "late" formation of solid Na_2O_2 observed by Ma et al.

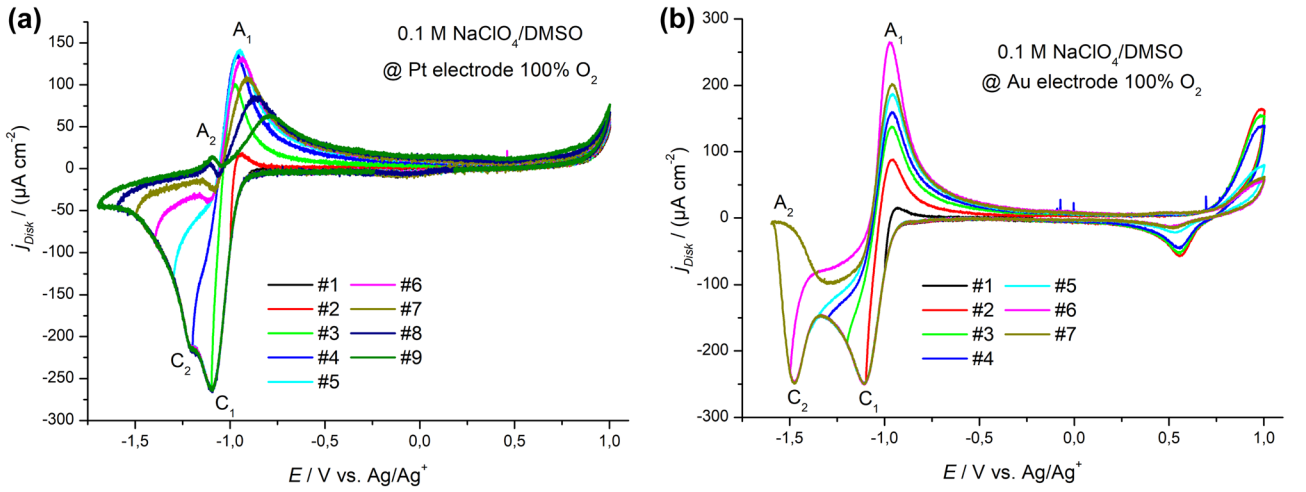

Fig. 2 CV study in a 0.1 M $NaClO_4$ in DMSO electrolyte saturated with 100% oxygen on (**a**) a Pt working electrode and (**b**) an Au working electrode at a constant sweep rate of 10 mV s^{-1} ($A = 0.164$ cm^2). The lower potential was reduced in 100 mV steps in every cycle. The electrolyte was saturated with 100% O_2

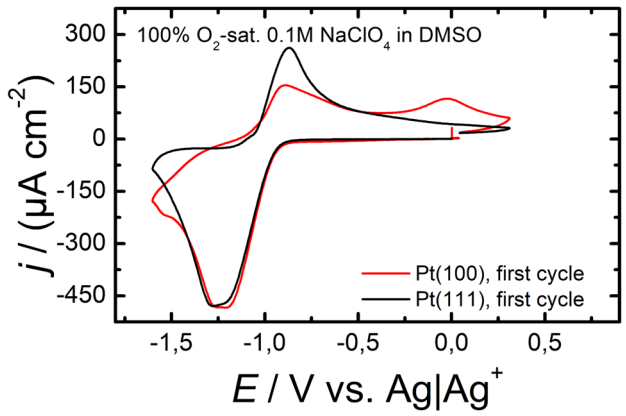

Fig. 3 Cyclic voltammetry of Pt(111) and Pt(100) at 50 mV s^{-1} in (100% O_2)-purged 0.1 M $NaClO_4$ vs $Ag|Ag^+$. The faradaic current is normalized to the geometric surface area. Shown is the first cycle respectively

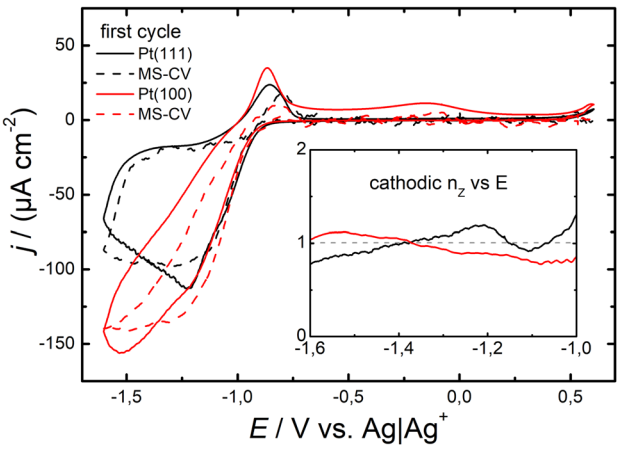

Fig. 4 Voltammetry (solid line) and MS-CVs (dashed line, mass 32) of Pt(100) (red) and Pt(111) (black) in (20% O_2 + 80% Ar)-purged 0.5 M $NaClO_4$ containing DMSO at 10 mV s^{-1} and 5 µl s^{-1} flow rate. The ion current in the MS-CV is normalized to the MS-calibration constant and thus refers to the same scale. Potential resolved number of transferred electrons is shown in the inset

is due to the necessary accumulation of peroxide. Also, the assumption of a second peak for the one electron reduction process is unreasonable, since the first peak C_1 is diffusion limited and 400 mV more negative the O_2 concentration in the vicinity of the electrode is zero; therefore, there is no O_2 available for reduction and a further charge flow (giving rise to a 2nd peak) is only possible if the superoxide is reduced to peroxide.

Galloway et al. published the cyclic voltammograms for Pt single-crystal electrodes in Na^+-containing DMSO combined with varied anions (in addition to their characterization of the reduction products by SHINERS). They observe a clear separation of peak C_1 and C_2 for Pt(111) and Pt(110) which they ascribe to the formation of a surface peroxide, but not at Pt(100) and pc Pt. In particular, the anodic oxidation peak A_2 is only visible for Pt(111) and Pt(110). Since these features resemble our measurements in 20% O_2, and also because their peak currents when using perchlorate are much lower than expected (542 µA cm^{-2} calculated from Randles–Sevcik equation for a reversible 1-e^- process; this corresponds to theoretically 242 µA cm^{-2} for 10 mV s^{-1} as compared to: 274 µA cm^{-2} in Fig. 2), we recorded the cyclic voltammograms for Pt(111) and Pt(100) under the conditions they used, in particular 100% O_2).

Figure 3 shows our result for the voltammetry of Pt(100) and Pt(111) under similar conditions. Concerning the voltammetry of Pt(100) and Pt(111), starting cathodic, the ORR starts at −0.9 V and the current density increases to a maximum at −1.25 V. After reaching the maximum, the current density decreases due to electrode deactivation by most likely the adsorbate layer of Na_2O_2. Continuing in anodic direction, the reduced oxygen species is reoxidized in one peak for Pt(111) and in two peaks for Pt(100). Comparing the single crystal results with those for the polycrystalline Pt (at 100% O_2 saturation and 10 mV s^{-1}) shows a similar overlapping of C_1 and C_2, which is more pronounced in Fig. 3, as the sweep rate is faster. During the OER peak A_2 cannot be observed in Fig. 3, which might also be due to the faster sweep rate. A clear difference is the appearance of the anodic peak close to 0.0 V vs $Ag|Ag^+$ for Pt(100). In an earlier publication [48], we found a similar behavior for Pt(100) in Li^+-containing DMSO. We have to mention that this feature at 0.0 V vanishes during the second cycle and was not observed by Galloway et al. under the same conditions. We further have to note that our results for Pt(111) in $Na(ClO_4)$ containing DMSO fit to the voltammetry Galloway et al. observed for Na(Otf) and Na(TFSI) containing DMSO, but not to what they found for $Na(ClO_4)$ containing DMSO. Furthermore, we were able to reproduce the second anodic peak close to 0.0 V for Pt(100) in a DEMS experiment under convection.

Figure 4 shows the DEMS experiment with calculated, potential resolved, and cathodic number of transferred electrons (n_z). The mass spectrometric cyclic voltammogram (MS-CV, dashed line) is directly comparable to the faradaic current (solid line), as the ion current was normalized to the MS calibration constant for O_2. Comparing Pt(111) with Pt(100), one observes an earlier deactivation of ORR for Pt(111). The absolute faradaic current in case of Pt(111) increases to a maximum close to −1.25 V and decreases continuously during the sweep. For Pt(100), the absolute current shows a shoulder close to −1.25 V and increases further up to a potential of −1.5 V. Even during the anodic sweep, no complete electrode deactivation is observed. Only a hysteresis hints to the formation of an (incomplete) blocking layer (of most likely adsorbed Na_2O_2). In case of

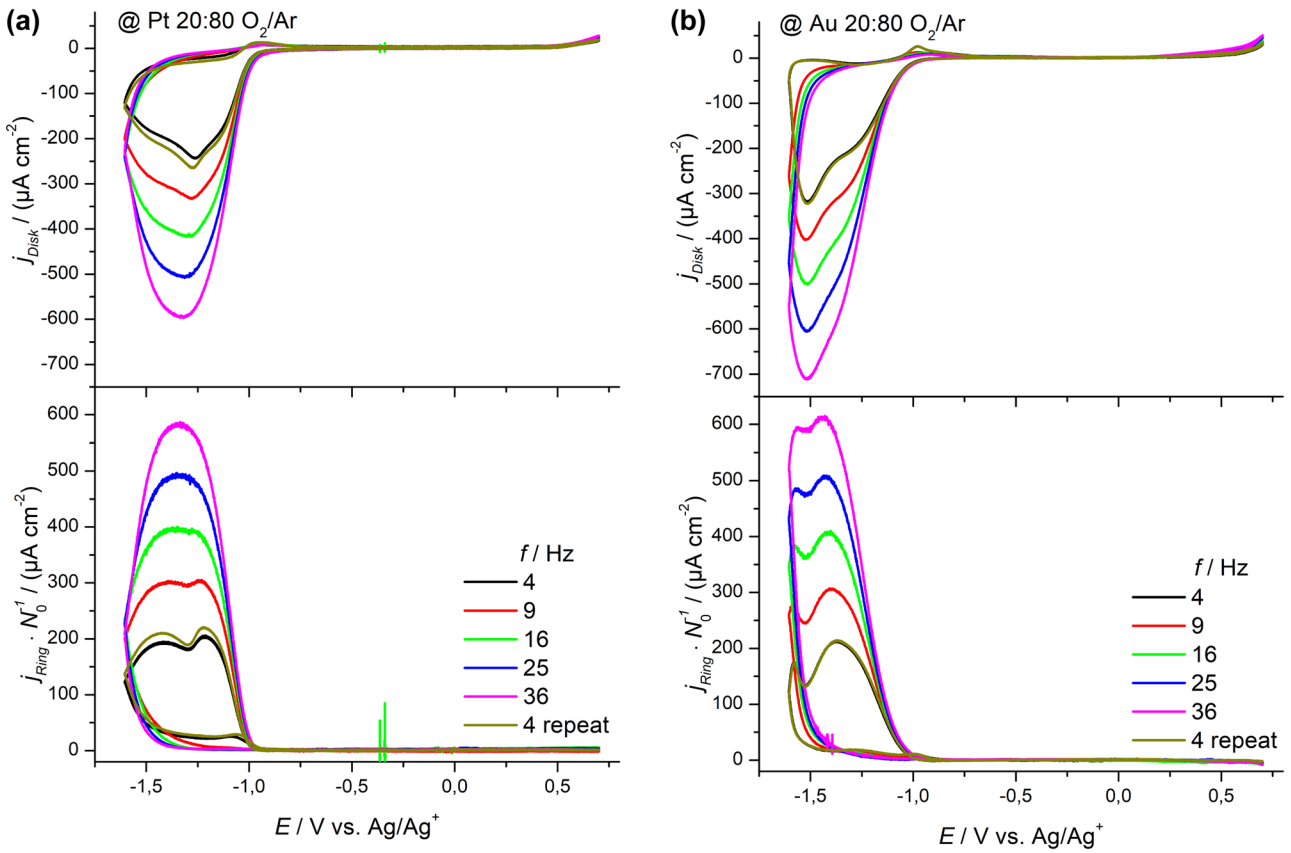

Fig. 5 RRDE studies in 0.1 M $NaClO_4$/DMSO with different rotation rates on (**a**) Pt ($R_F = 1.5$) and (**b**) Au ($R_F = 1.6$) ($A = 0.164$ cm^2). The electrolyte was saturated with a gas mixture containing 20% O_2 in Ar. The sweep rate was $v = 10$ mV s^{-1} and the ring potential was held at +0.3 V vs Ag|Ag$^+$ during all experiments. Disk-current is normalized to the geometrical surface area and ring-current is normalized to the theoretical collection efficiency (N_0) and geometrical surface area of the disk electrode

Pt(111), the OER is dominated by one peak close to −0.8 V due to reoxidation of superoxide, while in case of Pt(100), one observes in addition a peak at −0.2 V, probably due to reoxidation of an additional layer of peroxide, as the total OER charge density corresponds to approximately 2 ML of peroxide. Thus, we have to conclude that Pt(100) is more slowly blocked compared to Pt(111) and the complete reoxidation of the adsorbed/deposited ORR products requires higher potential. The formation of 2 ML peroxide exclusively on Pt(100) is also observed in Li^+-containing DMSO [48]. The number of transferred electrons during the ORR (around −1.2 V) further hints an earlier peroxide formation on Pt(111) compared to Pt(100), which might be the reason for the earlier electrode deactivation for Pt(111). Differently from the DEMS experiment with the pc Au electrode, the peroxide formation is less separated from the potential of superoxide formation; therefore, the change of the number of electrons is not clearly visible.

The ORR on both electrodes was also investigated using the RRDE. The CVs at different rotation rates are displayed in Fig. 5. The measurements on the Pt electrode (see Fig. 5a) and Au electrode (see Fig. 5b) show a decrease of the disc current at the most negative potentials instead of a diffusion limited plateau. This is due to the formation of an insulating layer of ORR products which is deposited on the electrode surfaces, which is well known for other metal-O_2 systems [10, 34, 49]. In the cyclic voltametric experiments in quiescent solution, this formation of a blocking layer is only observed for high O_2 concentrations, as discussed above (Fig. 2); at low O_2 concentration, formation of this blocking layer is too slow in the absence of convection. For the Au electrode, the transition between the 1 e$^-$ reduction and the 2 e$^-$ reduction at more negative potentials is clearly visible particularly at low rotation speed.

Correlating the ring and disc current according to Eq. (1), the potential dependent shares of superoxide can be calculated, as displayed in Fig. 6. It is seen that in the beginning of the ORR, on both electrodes the formation of superoxide is dominant (share of superoxide $x = 1$). During the cathodic sweep, the share of superoxide is undergoing a minimum on the Pt electrode at −1.3 V vs. Ag|Ag$^+$ for Pt (see Fig. 6a) and at −1.5 V vs. Ag|Ag$^+$ for Au. These minima are representing

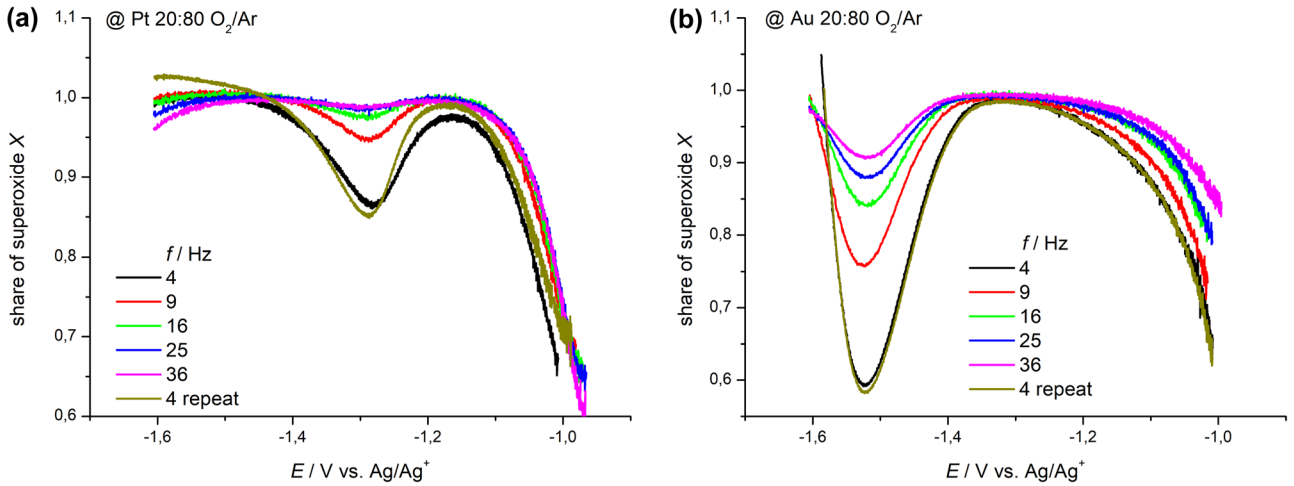

Fig. 6 Share of superoxide calculating by correlating the disc and ring current oft the RRDE measurements shown in Fig. 5 according to equation for the (**a**) Pt electrode and (**b**) Au electrode

the peroxide formation, which are in good agreement with the potentials for the observed peaks for the second electron transfer in the CVs without convection (see Fig. 1). This is confirmed by the DEMS measurement (Fig. S2) which shows a transition from the one-electron process to a second-electron transfer. For low rotation speed, the increased share of peroxide around 1.3 V shows up as a peak in the disc current and a minimum in the ring current (Fig. 5a). An increase of the rotation frequency results in an increase of the share of superoxide in the minima just mentioned because with increasing rotation frequency more superoxide is formed, whereas the amount of peroxide is surface—limited to a monolayer (of the DEMS experiment Fig. S2). We also observed a similar trend in a RRDE study on the ORR in Li^+ containing DMSO: after the peroxide formation, a transition to an increased share of superoxide formation was observed again [3, 27, 34, 50]. This process was explained by a geometrical effect: the formed peroxide blocks the electrode surface and thus the active centers on the electrode, which are necessary for peroxide formation. Therefore, the formation of superoxide starts again because of less requirements for surface sites. The extent of superoxide formation in this more negative potential region is larger in the Na^+ electrolyte. When the O_2 concentration is higher, peroxide formation and the blocking of the surface starts earlier, and so does the 2nd transition to superoxide formation, and the minima in the share of superoxide are less clear (see Fig. S5 and Fig. S6 in the supporting information for a measurement with 100% oxygen). Remarkable is the reappearance

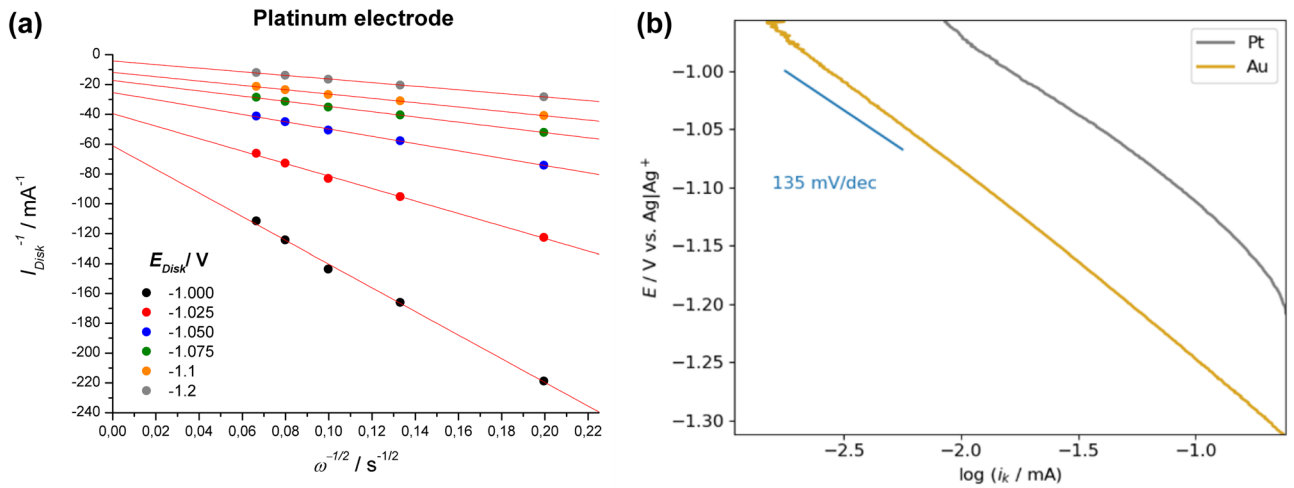

Fig. 7 (**a**) Exemplary Levich–Koutecký extrapolations for the Pt electrode at different disk potentials. (**b**) Generated Tafel plot using the determined kinetic currents from the Levich–Koutecký plot in (**a**). Shown are the Tafel lines for the experiments on Au and Pt

of oxygen reduction on Au in the anodic sweep similar to that in Fig. 2b which is less clear for 20% O_2.

In the onset of the ORR the blockage of the electrode surface with insoluble Na_2O_2 should be negligible, because of superoxide formation. Therefore, an analysis of the kinetic currents using the Levich–Koutecký equation should be possible here:

$$\frac{1}{I} = \frac{1}{I_K} + \frac{1}{I_D} = \frac{1}{I_K} + \frac{\nu^{\frac{1}{6}}}{0.62zFAD^{\frac{2}{3}}c\sqrt{\omega}} \tag{3}$$

Here, I is the disk current, I_K is the kinetic current, and I_D is the diffusion limited current. Furthermore, z is the number of transferred electrons, F is the Faraday constant, A is the geometric electrode surface, D is the diffusion coefficient of the electrochemically active species (here O_2), c is the concentration of O_2, and $\omega = 2\pi f$ denotes the angular rotation frequency of the RRDE. Equation (3) shows that with the help of a plot of $\frac{1}{I}$ as a function of $\omega^{-1/2}$ at the same disc potential, an extrapolation of I_K is possible. As an example, the Levich- Koutecký plot for the measurements on the platinum electrode is shown in Fig. 7a (for gold, it is shown in Fig. S7). The kinetic current I_K can be determined from the Levich–Koutecký plot, which can be used to determine the Tafel slope (see Fig. 7b). The Tafel slope shows a value of 135 mV dec^{-1} for the measurements on the Pt and Au electrode. These values (ideally 120 mV dec^{-1}) indicate that the first electron transfer (formation of superoxide) is the rate determining step in the ORR. As the potential is lowered, the Tafel slope is increasing particularly for Pt. This is due to the blockage of the electrode by the deposition of insulating Na_2O_2.

From the slope of the Levich–Koutecky plot, we determine the diffusion constants for oxygen and obtain $D(O_2) = 22.5 \cdot 10^{-6}$ cm^2 s^{-1} on Pt and ($D(O_2) = 23.4 \cdot 10^{-6}$ cm^2 s^{-1} for the Au electrode, in good agreement with the value of O_2 in 0.1 M $NaClO_4$ in DMSO determined by a nonelectrochemical method ($D(O_2) = 23.8 \cdot 10^{-6}$ cm^2 s^{-1} [51]) From the y-intercept of the Levich–Koutecky plot, the determination of the rate constant is possible with the following equation (A = geometric surface; F = Faraday constant; c_0^* = oxygen concentration).

$$k(E) = \frac{I_{disc}}{AFc_0^*} \tag{4}$$

For the determination of the rate constant, k_0, it is necessary to determine the equilibrium potential out of the half-wave-potential of the reduction peak (see supporting information Fig. S8). For the half-wave potential, the currents are used, which are obtained at a rotation rate of $f = 4$ Hz. (This low rotation frequency was used because diffusion limitation is most obvious here.) This potential is used to determine the equilibrium potential with the following equation and has a value for Pt of − 0.970 V (Au: $E_0 = -1.088$ V):

$$E_0 = E_{1/2} + \frac{RT}{F} ln\left(\left(\frac{D(O_2)}{D(O_2^-)} \right)^{2/3} \right) \tag{5}$$

The k_0 values which we get from the Levich–Koutecký analysis are for the Pt electrode $k_0 = 3.77 \cdot 10^{-3}$ cm s^{-1} and for the Au electrode $k_0 = 0.46 \cdot 10^{-3}$ cm s^{-1}. (Strictly speaking, this k_0 (and E_0) refer to the equilibrium potential at which the concentration of superoxide is identical to the oxygen concentration, whereas the true standard equilibrium potential refers to the standard state, which is an activity of 1 M for superoxide and 1 bar for oxygen, corresponding to a concentration of 1.85 mM.)

Using this information and the shown CVs without convection at different sweep rates (see Fig. S3 in the supporting information), a further kinetic analysis of the redox system (O_2/O_2^-) is possible. The sweep rate dependency of the peak positions shows especially on the Au electrode a huge shift compared to the experiments on the Pt electrode. Therefore, we used this behavior to analyze the kinetics of the O_2/O_2^- redox couple on both electrodes. The redox couple formed by C_1 and A_1 (see Fig. 1) can be used for the heterogeneous kinetical analysis from Lavagnini and Nicholson [52] [47]. The evaluation results in a slope of 3.98 (mV s^{-1})$^{0.5}$ for the measurements on the Pt electrode and 0.43 (mV s^{-1})$^{0.5}$ for the measurements on the Au electrode (see supporting information Fig. S9b)). Using Eq. (2) (see supporting information) gives a k_0 of 0.40·10^{-3} cm s^{-1} for the Au electrode and 3.79 10^{-3} cm s^{-1} for the Pt electrode. We have already performed the same analysis in a previous publication for the O_2/O_2^- redox couple in K^+ containing DMSO [47]. A comparison with the values determined

Table 2 Comparison of the $k_0(O_2/O_2^-)$ values in the electrolytes

	Na^+		K^+[47]	
$k_0(O_2/O_2^-)$	Pt	Au	Pt	Au
Levich–Koutecký	$3.77 \cdot 10^{-3}$ cm s^{-1}	$0.46 \cdot 10^{-3}$ cm s^{-1}	$5.7 \cdot 10^{-3}$ cm s^{-1}	$1.28 \cdot 10^{-3}$ cm s^{-1}
Lavagnini	$3.79 \cdot 10^{-3}$ cm s^{-1}	$0.40 \cdot 10^{-3}$ cm s^{-1}	$4.06 \cdot 10^{-3}$ cm s^{-1}	$0.94 \cdot 10^{-3}$ cm s^{-1}

here shows that the two systems are comparable (Table 2). The heterogeneous rate constant is smaller on Au than on Pt. Furthermore, the determined values of k_0 show a good agreement regarding the order of magnitude. This comparison shows that k_0 is influenced more strongly by the electrode material than by the cation in the electrolyte.

The ORR in Li^+/Na^+ Mixed Electrolytes

We investigated the influence of Li^+ on the ORR and OER in the Na^+-containing electrolyte by partially substituting $NaClO_4$ by $LiClO_4$. The ionic strength of the electrolyte was kept constant at 0.1 M. A CV study for the electrode materials Pt and Au is shown in Fig. 8.

At the Pt electrode (Fig. 8a), the peak C_2 disappears with an increase of the Li^+ content. However, the absolute current of peak C_1 does not change much. At the Au electrode (Fig. 8b), peak C_2 increases with very small additions of Li^+ and then shifts in positive direction. For both electrodes, peak A_1 corresponding to superoxide oxidation diminishes even after addition of 0.1% Li^+. Instead, re-oxidation peaks evolve at larger overpotentials. An interpretation of this effect is possible with the help of further RRDE measurements (see Fig. 9).

The RRDE measurements in Fig. 9a show that by increasing the Li^+ content in the electrolyte, the flowing electrical charge required to block the electrode decreases. Thus, the flowing charge in the ORR (between the onset of ORR and the negative potential limit in both, cathodic and anodic direction) is 2451 µC for the pure Na^+-containing electrolyte, 1570 µC for the mixture 62:1 Na^+:Li^+ and 844 µC for the pure Li^+-containing electrolyte. Increasing the amount of Li^+ in the electrolyte results in a shift of peroxide formation to more positive potentials and, more importantly, more severe blocking, as also visible from the lower ring currents. Li_2O_2 is well known to effectively block the electrode [3] [46] as opposed to Na_2O_2 (cf. the RRDE results above), and Li_2O_2 is formed at more positive potentials than Na_2O_2; therefore, it is indeed expected that the electrode is blocked earlier. The experiment shows that this is the case even for very low concentrations of Li^+. Its concentration of 0.1 mM is comparable to the oxygen concentration in this electrolyte of approximately 0.4 mM for 20% saturation. Therefore, as soon as the Li^+ concentration is sufficient to completely react with oxygen during its reduction, the formation of Li_2O_2 is the dominating reaction. (Strictly speaking, the diffusion rates of O_2 and Li^+ toward the surface would have to be comparable.) The transition from Na^+-dominated to Li^+-dominated mechanism also explains the small changes in peak C_1 with increasing Li^+ concentration in Fig. 8 (CV in quiescent solution): superoxide formation occurs at a very similar potential for both cations, but only for Li^+ the peroxide formation is occurring in parallel at Pt. The slight increase in C_1 current therefore is due to the additional contribution of the 2 e^- process, which however is not a purely diffusion controlled, but also surface limited process because of the adsorbate character in the case of Li^+. In the case of Au, superoxide formation and peroxide formation are well separated even in the case of pure Li^+ electrolyte and therefore peak C_2 does not vanish [27]. Also, the shift of the minimum in superoxide share in Fig. 10b (maximum in peroxide formation) which is caused by the transition from the superoxide to peroxide formation and then again to superoxide formation to more

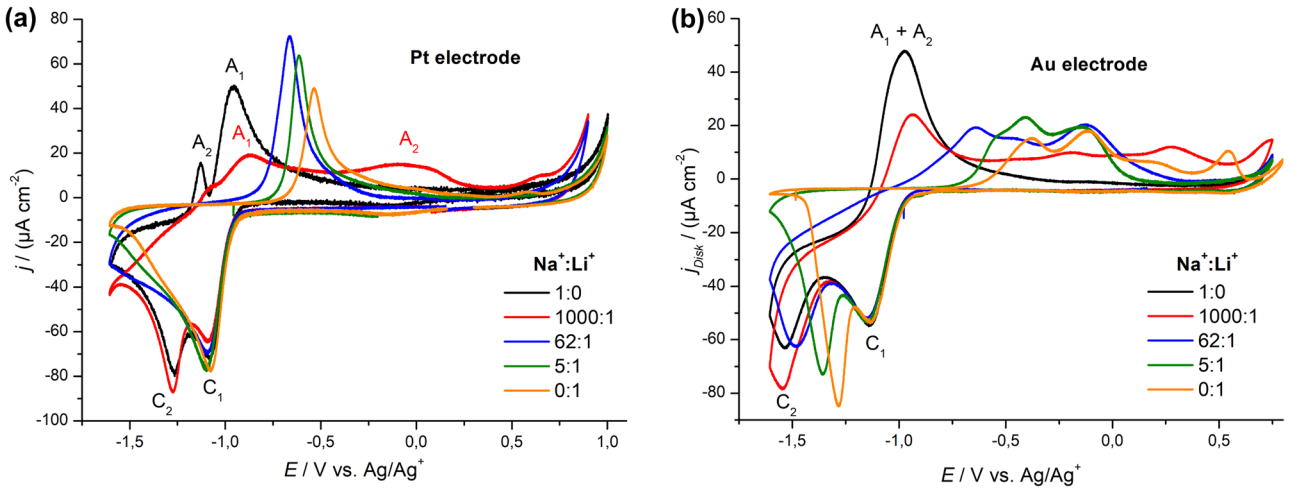

Fig. 8 CV measurements with different mixtures of the conducting salts $LiClO_4$ and $NaClO_4$ in DMSO. The mixing ratios are shown in the figures and correspond to Li^+ concentrations of 0, 0.1, 1.6, 19.2, and 100 mM. The ionic strength was kept constant at 0.1 M. The measurements were performed (**a**) on a Pt electrode and (**b**) on an Au electrode ($A = 0.164$ cm^2). The sweep rate was 10 mV s^{-1} and the electrolyte was saturated with a 20:80 mixture O_2: Ar (corresponding to an O_2-concentration of 0.37 mM [51]

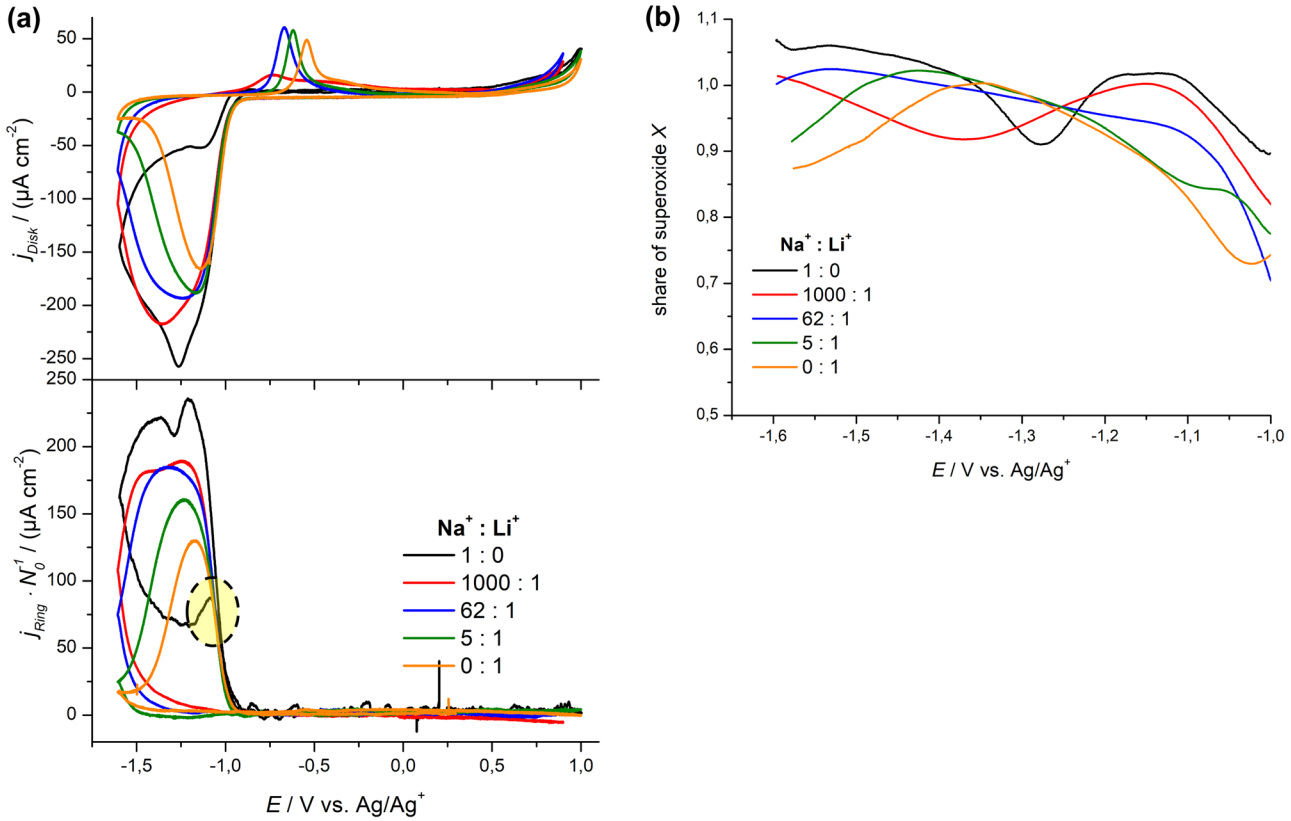

Fig. 9 (**a**) RRDE study with a Pt electrode (A = 0.164 cm^2) with various mixtures of $NaClO_4$ and $LiClO_4$ in DMSO. The rotation frequency was 4 Hz, and the sweep rate was v = 10 mV s^{-1}. The ring potential was held at 0.3 V. (**b**) Calculated share of superoxide *x* for the measurements shown in (**a**). Disk-current is normalized to the geometrical surface area and ring-current is normalized to the theoretical collection efficiency (N_0) and geometrical surface area of the disk electrode

positive potentials is due to the change from Na^+-dominated to Li^+-dominated ORR.

Concerning the OER, already the CVs without rotation in Fig. 8 show that the O_2/O_2^- redox pair, which is fairly reversible in 0.1 M $NaClO_4$ DMSO (peaks C_1 and A_1), becomes irreversible by small amounts of Li^+ in the electrolyte. With convection, already in presence of the smallest Li^+ content, re-oxidation currents, which are hardly visible in pure Na^+ electrolyte, indicate the presence of peroxide adsorbed or deposited on the surface.

The reason for this is that superoxide is less stable in the presence of Li^+ [31, 53] and therefore is quickly further reduced to peroxide [3], whereas NaO_2 dissolved in DMSO is kinetically stable [31] and only further reduced at lower potentials, as also visible in the shifted reduction peaks. (Since superoxide is detected at the ring electrode also in presence of Li^+, the disproportionation reaction to peroxide and oxygen[31, 53] obviously occurs on a timescale lager than 1 s as this time corresponds to the transfer time of a soluble species between the disc electrode and the ring electrode at 4 Hz. The reversibility of the reduction to LiO_2 is also visible in cyclic voltammetry if the potential is reversed at a high enough potential (cf. Fig. S12).

When only Na^+ ions are present, the blocking peroxide is also formed, but reoxidized at potentials below the onset of superoxide formation, cf. peak A_2 in the CVs without convection (Figs. 1, 9). This is also confirmed in the RRDE experiments (Figs. 10, 11) where for Au the shoulder in both disc and ring current indicates continuous superoxide formation and any hysteresis disappears around the onset potential. In the case of Pt, even a small positive peak due to reoxidation of peroxide is superimposed to the reductive disc current and a peak in the ring current indicates increased superoxide formation due to peroxide oxidation.

Peaks in the OER region shift to more positive potentials as the Li^+ content is increased in the electrolyte. It is noticeable that on the Au electrode as well as on the Pt electrode for a mixture of 1000:1 Li^+:Na^+ a similar shape in the CV is observed in the potential range of the OER. There a wide OER region with small Faraday currents is observed. It is conceivable that a mixed lithium/sodium peroxide phase, which shows kinetic inhibition in

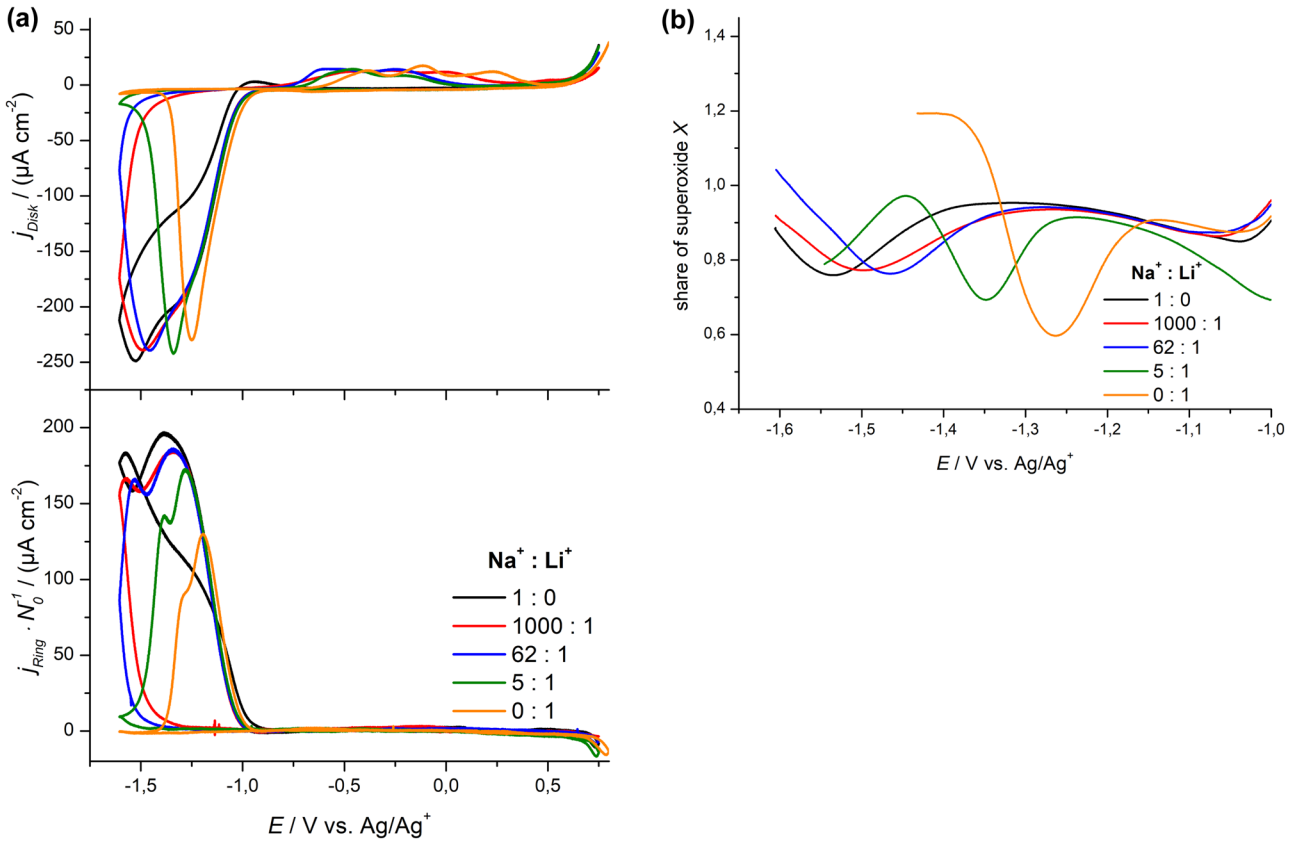

Fig. 10 (**a**) RRDE study with an Au electrode (A = 0.164 cm^2) with various mixtures of $NaClO_4$ and $LiClO_4$ in DMSO. The rotation frequency was 4 Hz and the sweep rate was v = 10 mV s^{-1}. The ring potential was held at 0.3 V. (**b**) Calculated share of superoxide *x* for the measurements shown in (**a**). Disk-current is normalized to the geometrical surface area and ring-current is normalized to the theoretical collection efficiency (N_0) and geometrical surface area of the disk electrode

its electrochemical oxidation, is formed in this electrolyte. If the Li^+ content in the electrolyte is further increased, the onset of the OER shifts further to positive potentials. On the Pt electrode, oxidation of the peroxide occurs in a peak shifting positively with increasing Li^+ concentration. On the Au electrode, however, the known shape of the OER region in Li^+-containing DMSO occurring in several peaks is observed. The reason for the appearance of multiple peaks in the OER on Au electrodes is still not completely understood [27, 54].

Using the RRDE measurements, it is possible to calculate the relative contribution of the disk current $i_{surface}$ responsible for the deposition/adsorption of ORR products (mainly peroxide) on the disk electrode and its oxidation. This will additionally illuminate and summarize what is said above. $i_{surface}$ can be calculated using the following expression:

$$i_{surface} = i_{Disk} - \frac{i_{Ring}}{N_0} \tag{6}$$

Herein, i_{Disk} is the disk current, i_{Ring} the ring current and N_0 the theoretical collection efficiency of the RRDE electrode. The disc current for soluble (and oxidizable) species ($i_{soluable}$) is calculated according to:

$$i_{soluable} = -\frac{i_{Ring}}{N_0} \tag{7}$$

Figure 11 shows the calculated values of $i_{surface}$ and $i_{soluable}$ as a function of the disk potential are shown for the RRDE measurements in the Li^+/Na^+ mixture already shown in Figs. 9, 10.

For the pure $NaClO_4$-containing electrolyte, the CVs of $i_{surface}$ are showing a peak in the ORR on the Pt and Au electrode (see black dotted lines in Fig. 11). The peak potential correlates with the second ORR peak (peak C_2 in Fig. 1) in the CV without convection and can therefore be assigned to the peroxide formation. By increasing the Li^+ content in the electrolyte, the peroxide formation shifts to higher potentials. This effect is expected because the redox potential of Li_2O_2 formation is shifted about 200 mV positively

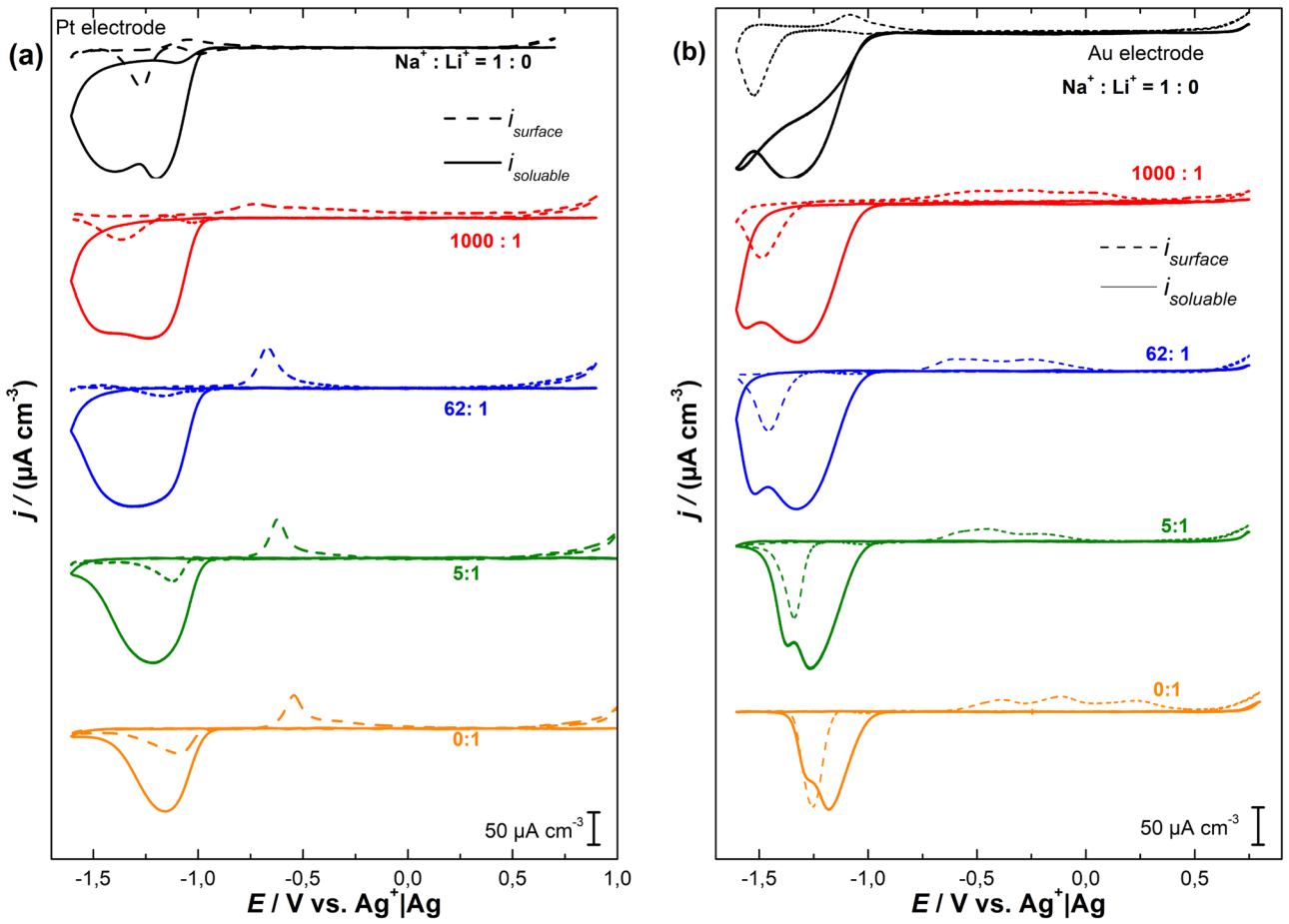

Fig. 11 Calculated currents for the deposition f solid products on the surface $i_{surface}$ and for the RRDE data shown in Figs. 9, 10 for (**a**) the Pt electrode and (**b**) the Au electrode

compared to Na_2O_2 formation (see redox potentials in the introduction). (An exception is the case of 0.1% Li^+, where at Pt the superoxide is formed negative of Na_2O_2 formation and where reoxidation is also occurring at more positive potentials than in the other cases, possibly because of the formation of a mixed Li-Na-oxide.) Experimentally, we observe a positive shift of the peroxide formation from a pure Na^+-containing electrolyte to a pure Li^+-containing electrolyte of 200 mV on the Pt electrode and 240 mV on the Au electrode. In general, the peroxide is kinetically less stable on the Pt electrode relative to the Au electrode, which shows the earlier onset of peroxide formation on the Pt electrode and its earlier reoxidation. In fact, the peroxide formation on Pt electrode shifts to the ORR onset, whereas on Au electrode, the peroxide formation is well separated from the superoxide formation and starts thereafter. Furthermore, the absolute peak current in $i_{surface}$ increases with an increase of the Li concentration on the Au electrode. On the Pt electrode, no clear increase of the peak current is observed. A possible explanation for this is that on Au electrodes a parallel, direct reduction of oxygen to peroxide is possible without forming a soluble reaction intermediate (soluble superoxide). This reaction channel was not found on Pt electrodes and is probably the reason for the difference described above [34].

For the electrolyte systems with higher Li^+ content, the decrease of the peroxide current of $i_{surface}$ correlates with a blockade of the electrode, which is therefore no longer active for ORR. This can be recognized by a drop of $i_{soluable}$ after $i_{surface}$ has dropped to the baseline. A different behavior is observed in the Na^+ containing electrolyte with a low Li^+ content: there, the current of $i_{soluable}$ can be maintained even after the electrode is blocked with peroxide. This suggests a more porous or defect rich structure of the deposited layer through which mass transport can occur. On the Au electrode $i_{soluable}$ is even split into two peaks. The peak at more negative potentials is observed just after $i_{surface}$ has described its maximum. Thus, this second peak can be assigned to a second mechanism of superoxide formation, namely the reduction of oxygen on the peroxide layer, while the continuous drop in current further indicates that superoxide formation is only

possible as long as the peroxide layer is incomplete. Due to the positive potential shift of the reduction peak in $i_{surface}$ by increasing the Li^+ concentration, the blockage of the electrode occurs earlier in the sweep, which also ends up in earlier collapse of $i_{soluable}$.

In general, we observed a higher charge for the formation of the surface species (integration of of $i_{surface}$) on the Au electrode than on the Pt electrode. The mean value of the charge on the Pt electrode 780 µC cm^{-2} and 1300 µC cm^{-2} on the Au electrode (normalized to the real surface area of the electrocatalyst, corresponding to 1.2 and 2.1 ML, cf. Table S1). There is no clear trend for the dependence on the Li^+ content. These values are very comparable to the charges for reoxidation of the adsorbed peroxide (average for the Li^+ containing electrolytes 640 µC cm^{-2} and 1060 µC cm^{-2}, corresponding to 1.3 and 1.7 ML), except for the pure Na^+ electrolyte in which the peroxide is reoxidized in the potential range of superoxide formation already. We already observed the capability of an Au electrode to host about twice the amount of Li_2O_2 compared to a Pt electrode in an earlier study [27].

Conclusion

Using cyclic voltammetry and the rotating ring disc electrode, we investigated the ORR and OER Na^+ containing DMSO, as well as in Li^+-Na^+ mixed electrolytes. We focused on a comparison between the electrode materials Pt and Au. For the pure Na^+ electrolyte, we could make the following observations:

- In the onset of the ORR mostly superoxide is formed. The analysis of the rotational dependency of the share of superoxide in the region of peroxide formation indicated soluble superoxide as reaction intermediate.
- On Pt and Au electrode, the first electron transfer (formation of superoxide) is the rate determining steps as indicated by a Tafel slope of 135 mV dec^{-1}.
- The heterogeneous rate constant for the redox couple O_2/O_2^- is determined from Levich-Koutecký-plots and with the Nicholson-Lavagnini-Methode in Na^+ and K^+ containing DMSO and summarized in Table 2.
- Formation of the surface blocking Na_2O_2 is faster on the Pt surface than on the Au surface and therefore formed at higher electrode potentials (lower overpotentials).
- Superoxide continues being formed on the initially defect rich or porous peroxide layer before it is slowly becoming completely blocking.
- Reoxidation of Na_2O_2 is much more reversible than that of Li_2O_2 and occurs already in the potential range of ORR to superoxide, thus leading to superoxide.
- Peroxide formation occurs to a smaller extent on the single crystal electrodes of Pt. Blocking is more slowly on Pt(100) than on Pt(111), but the peroxide also seems more stable.

By adding Li^+ to the electrolyte, we found:

- The ORR and OER show a transition from Na^+-dominated to Li^+-dominated mechanism as soon as the Li^+ concentrations reaches the magnitude of O_2 concentration: the redox couple O_2/O_2^- seems to become less reversible, which is due to the earlier blocking of the electrode surface by peroxide, which is more stable and re-oxidized only at much higher potentials than in pure Na^+ electrolyte.
- With the help of the RRDE measurements the CV was deconvoluted into a current responsible for the formation of solid product on the disc electrode (peroxide) and the formation of soluble products (superoxide). By doing so, we could demonstrate that:
    - With a higher Li^+ content in the electrolyte the peroxide formation is shifting to more positive potentials, which is an expected effect according to the available thermodynamic data.
    - The reduction of oxygen to superoxide on the peroxide layer becomes visible as a peak in the current distribution for the formation of soluble products parallel or even after the formation of peroxide has reached its maximum. It is maintained as long as the peroxide layer is incomplete or defect rich, which is the more the case, the lower the Li^+ content is.
    - The amount of peroxide formed is rather independent of the Na^+ to Li^+ ratio in the DMSO electrolyte.

Supplementary Information The online version contains supplementary material available at https://doi.org/10.1007/s12678-021-00669-4.

Funding Open Access funding enabled and organized by Projekt DEAL. This work is funded by the Federal Ministry of Education and Research (BMBF). This work is part of the LiBaLu-project in the framework of the "Vom Material zur Innovation"-initiative (03XP0029A).

References

1. S. Zhao, B. Qin, K.-Y. Chan, C.-Y.V. Li, F. Li, Batteries Supercaps **2**, 725 (2019)
2. G. Girishkumar, B. McCloskey, A.C. Luntz, S. Swanson, W. Wilcke, J. Phys. Chem. Lett. **1**, 2193 (2010)
3. C.J. Bondue, M. Hegemann, C. Molls, E. Thome, H. Baltruschat, J. Electrochem. Soc. **163**, A1765 (2016)
4. B.D. McCloskey, R. Scheffler, A. Speidel, G. Girishkumar, A.C. Luntz, J. Phys. Chem. C **116**, 23897 (2012)
5. C.O. Laoire, S. Mukerjee, E.J. Plichta, M.A. Hendrickson, K.M. Abraham, J. Electrochem. Soc. **158**, A302 (2011)
6. Q. Sun, Y. Yang, Z.-W. Fu, Electrochem. Commun. **16**, 22 (2012)
7. G. Gritzner, J. Mol. Liq. **156**, 103 (2010)
8. H. Yadegari, C.J. Franko, M.N. Banis, Q. Sun, R. Li, G.R. Goward, X. Sun, The Journal of Physical Chemistry Letters **8**, 4794 (2017)
9. P. Reinsberg, C. Bondue, H. Baltruschat, Electrochim. Acta **200**, 214 (2016)
10. P. Reinsberg, C.J. Bondue, H. Baltruschat, J. Phys. Chem. C **120**, 22179 (2016)
11. P. Reinsberg, A.A. Abd-El-Latif, H. Baltruschat, Electrochim. Acta **273**, 424 (2018)
12. W.-W. Yin, Z.-W. Fu, ChemCatChem **9**, 1545 (2016)
13. E. Peled, D. Golodnitsky, H. Mazor, M. Goor, S. Avshalomov, J. Power Sources **196**, 6835 (2011)
14. B.L. Ellis, L.F. Nazar, Curr. Opin. Solid State Mater. Sci. **16**, 168 (2012)
15. P. Hartmann, C.L. Bender, J. Sann, A.K. Durr, M. Jansen, J. Janek, P. Adelhelm, Phys. Chem. Chem. Phys. **15**, 11661 (2013)
16. P. Hartmann, C.L. Bender, M. Vra ar, A.K. Dürr, A. Garsuch, J.r. Janek, P. Adelhelm, Nat. Mater. **12**, 228 (2013)
17. J. Kim, H.-D. Lim, H. Gwon, K. Kang, Phys. Chem. Chem. Phys. **15**, 3623 (2013)
18. C.L. Bender, P. Hartmann, M. Vračar, P. Adelhelm, J. Janek, Adv. Energy Mater. **4**, 1301863 (2014)
19. C. Xia, R. Black, R. Fernandes, B. Adams, L.F. Nazar, Nat. Chem. **7**, 496 (2015)
20. E. Faktorovich-Simon, A. Natan, E. Peled, D. Golodnitsky, J. Solid State Electrochem. **22**, 1015 (2018)
21. J. Kim, H. Park, B. Lee, W.M. Seong, H.-D. Lim, Y. Bae, H. Kim, W.K. Kim, K.H. Ryu, K. Kang, Nat. Commun. **7**, 10670 (2016)
22. I.M. Aldous, L.J. Hardwick, Angew. Chem. Int. Ed. **55**, 8254 (2016)
23. D. Schröder, L. Bender Conrad, R. Pinedo, W. Bartuli, G. Schwab Matthias, Z. Tomovic, J. Janek, Energy Technol. **5**, 1242 (2016)
24. S. Kang, Y. Mo, S.P. Ong, G. Ceder, Nano Lett. **14**, 1016 (2014)
25. C.L. Bender, D. Schröder, R. Pinedo, P. Adelhelm, J. Janek, Angew. Chem. Int. Ed. **55**, 4640 (2016)
26. I. Landa-Medrano, I. Ruiz de Larramendi, T.f. Rojo, Electrochim. Acta. **263**, 102 (2018)
27. C. Bondue, P. Reinsberg, A.A. Abd-El-Latif, H. Baltruschat, Phys. Chem. Chem. Phys. **17**, 25593 (2015)
28. V.S. Dilimon, C. Hwang, Y.-G. Cho, J. Yang, H.-D. Lim, K. Kang, S.J. Kang, H.-K. Song, Sci. Rep. **7**, 17635 (2017)
29. S. Ma, W.C. McKee, J. Wang, L. Guo, M. Jansen, Y. Xu, Z. Peng, Phys. Chem. Chem. Phys. **19**, 12375 (2017)
30. L. Johnson, C. Li, Z. Liu, Y. Chen, S.A. Freunberger, P.C. Ashok, B.B. Praveen, K. Dholakia, J.-M. Tarascon, P.G. Bruce, Nat. Chem. **6**, 1091 (2014)
31. C. Sheng, F. Yu, Y. Wu, Z. Peng, Y. Chen, Angew. Chem. Int. Ed. **130**, 10054 (2018)
32. T.A. Galloway, J.C. Dong, J.F. Li, G. Attard, L.J. Hardwick, Chem. Sci. **10**, 2956 (2019)
33. C.J. Bondue, P.P. Bawol, A.A. Abd-El-Latif, P. Reinsberg, H. Baltruschat, J. Phys. Chem. C **121**, 8864 (2017)
34. P. Reinsberg, A. Weiss, P.P. Bawol, H. Baltruschat, J. Phys. Chem. C **121**, 7677 (2017)
35. L. Schafzahl, N. Mahne, B. Schafzahl, M. Wilkening, C. Slugovc, M. Borisov Sergey, A. Freunberger Stefan, Angew. Chem. **129**, 15934 (2017)
36. H.M.A. Amin, C. Molls, P.P. Bawol, H. Baltruschat, Electrochim. Acta **245**, 967 (2017)
37. A.J. Bard, L.R. Faulkner, *Electrochemical Methods: Fundamentals and Applications* (John Wiley & Sons Inc., New York, Weinheim, 2001).
38. A.A. Abd-El-Latif, H. Baltruschat, in *Encyclopedia of Applied Electrochemistry*. ed. by G. Kreysa, K.-I. Ota, R. Savinell (Springer, New York Dordrecht Heidelberg London, 2014), p. 507
39. A.A. Abd-El-Latif, C.J. Bondue, S. Ernst, M. Hegemann, J.K. Kaul, M. Khodayari, E. Mostafa, A. Stefanova, H. Baltruschat, TrAC, Trends Anal. Chem. **70**, 4 (2015)
40. H. Baltruschat, in *Interfacial Electrochemistry*. ed. by A. Wieckowski (Marcel Dekker Inc, New York, Basel, 1999), p. 577
41. H. Baltruschat, J. Am. Soc. Mass Spectrom. **15**, 1693 (2004)
42. P.H. Reinsberg, A. Koellisch, P.P. Bawol, H. Baltruschat, Phys. Chem. Chem. Phys. **21**, 4286 (2019)
43. A. Cuesta, L.A. Kibler, D.M. Kolb, J. Electroanal. Chem. **466**, 165 (1999)
44. L.A. Kibler, Preparation and Characterization of Noble Metals Single Crystal Electrodes, University of Ulm (2003)
45. A.S. Shatla, A.A. Abd-El-Latif, S. Ayata, D. Demir, H. Baltruschat, Electrochim. Acta **334**, 135556 (2020)
46. A. Koellisch-Mirbach, H. Baltruschat, In preparation, (2021).
47. P.H. Reinsberg, A. Koellisch, H. Baltruschat, Electrochim. Acta **313**, 223 (2019)
48. A. Koellisch-Mirbach, T. Lohrmann, P.H. Reinsberg, H. Baltruschat, J. Electroanal. Chem. **875**(2020), 114560 (1959)
49. P.P. Bawol, J.H. Thimm, H. Baltruschat, ChemElectroChem **6**, 6038 (2019)
50. Q. Yu, S. Ye, J. Phys. Chem. C **119**, 12236 (2015)
51. P.H. Reinsberg, P.P. Bawol, E. Thome, H. Baltruschat, Anal. Chem. **90**, 14150 (2018)
52. I. Lavagnini, R. Antiochia, F. Magno, Electroanalysis **16**, 505 (2004)
53. E. Mourad, Y.K. Petit, R. Spezia, A. Samojlov, F.F. Summa, C. Prehal, C. Leypold, N. Mahne, C. Slugovc, O. Fontaine, S. Brutti, A. Freunberger Stefan, Energy Environ. Sci. **12**, 2559 (2019)
54. C. Liu, S. Ye, J. Phys. Chem. C **120**, 25246 (2016)